Research article

In vitro cytotoxic activity on KATO-III cancer cell lines of mangiferolic acid purified from Thai *Tetragonula laeviceps* propolis

Thitipan Meemongkolkiat [a], Songchan Puthong [b], Phanthiwa Khongkarat [a], Preecha Rod-im [c], Orawan Duangphakdee [c], Packapong Tuthaisong [d], Preecha Phuwapraisirisan [d], Chanpen Chanchao [a,*]

[a] *Department of Biology, Faculty of Science, Chulalongkorn University, 254 Phayathai Road, Bangkok, 10330, Thailand*
[b] *Institute of Biotechnology and Genetic Engineering, Chulalongkorn University, 254 Phayathai Road, Bangkok, 10330, Thailand*
[c] *Native Honeybee and Pollinator Research Center, Ratchaburi Campus, King Mongkut's University of Technology Thonburi, Ratchaburi, 70150, Thailand*
[d] *Center of Excellence in Natural Products, Department of Chemistry, Faculty of Science, Chulalongkorn University, 254 Phayathai Road, Bangkok, 10330, Thailand*

A B S T R A C T

Gastric cancer is a global health concern, but current treatment with chemotherapy and surgery is often inadequate, prompting the exploration of alternative treatments. Propolis is a natural substance collected by bees known for its diverse properties linked to floral sources. The Dichloromethane Partitioned Extract (DPE) from *Tetragonula laeviceps* propolis, in Bankha district, Thailand was previously shown to possess significant cytotoxicity against KATO-III gastric cancer cells, while showing lower cytotoxicity toward WI-38 normal fibroblast cells. Here, the DPE was further fractionated by column chromatography, identified active fractions, and subjected to structural analysis using nuclear magnetic resonance spectroscopy. Cytotoxicity against KATO-III cells was reevaluated, and programmed cell death was analyzed using flow cytometry. Expression levels of cancer-related genes were measured using quantitative real-time reverse transcriptase PCR. Cardol C15:2 (compound **1**) and mangiferolic acid (MF; compound **2**) were discovered in the most active fractions following structural analysis. MF exhibited strong cytotoxicity against KATO-III cells (IC_{50} of 4.78–16.02 μg/mL), although this was less effective than doxorubicin (IC_{50} of 0.56–1.55 μg/mL). Morphological changes, including decreased cell density and increased debris, were observed in KATO-III cells treated with 30 μg/mL of MF. Significant induction of late-stage apoptosis and necrosis, particularly at 48 and 72 h, suggested potential DNA damage and cell cycle arrest, evidenced by an increased proportion of sub-G1 and S-phase cells. Doxorubicin, the positive control, triggered late apoptosis but caused more necrosis after 72 h. Furthermore, MF at 30 μg/mL significantly increased the expression level of *COX2* and *NFκB* genes linked to inflammation and cell death pathways. This upregulation was consistent at later time points (48 and 72 h) and was accompanied by increased expression of *CASP3* and *CASP7* genes. These findings suggest MF effectively induces cell death in KATO-III cells through late apoptosis and necrosis, potentially mediated by upregulated inflammation-related genes.

* Corresponding author.
E-mail addresses: lek_tues_ti@hotmail.com (T. Meemongkolkiat), songchan.p@chula.ac.th (S. Puthong), parephanthiwa@gmail.com (P. Khongkarat), preecha.rodim@mail.kmutt.ac.th (P. Rod-im), orawan.dua@kmutt.ac.th (O. Duangphakdee), 1997chemistry@gmail.com (P. Tuthaisong), preecha.p@chula.ac.th (P. Phuwapraisirisan), chanpen.c@chula.ac.th (C. Chanchao).

1. Introduction

Stomach cancer is the fifth most common cancer worldwide and is particularly prevalent in Asian countries and some Western nations. The Global Cancer Observatory (GCO) reported in the GCO website (gco.iarc.fr) that around 10 million deaths from cancer in 2020, although rates are declining due to the control and prevention of risk factors and the promotion of healthy habits [1]. Nevertheless, gastric cancer remains a pressing global health issue with varying risk factors depending on the cancer's location and type [2]. Despite advancements in surgery, chemotherapy, and other treatments, adverse side effects such as multidrug resistance or the requirement for post-surgery chemotherapy have been documented [3]. Typical chemotherapy drugs for gastric cancers, including 5-fluorouracil (5-Fu), cisplatin (DDP), paclitaxel, and epirubicin, are utilized. Nevertheless, the efficacy of chemotherapy is constrained, with gastric cancer's 5-year overall survival rate standing at just approximately 27.4 % [4]. Consequently, researchers are exploring alternative treatments to the traditional chemotherapy and surgery, focusing on targeted therapeutic approaches.

More attention has been directed towards compounds derived from natural sources, regarded as promising agents with reduced side effects, to advance cancer treatment outcomes. Natural products have long been a focus for effective treatments for various diseases, including cancer [5]. One of the natural substances currently attracting attention is propolis, a resinous material made by bees from plant sources. Propolis is widely recognized for its wide range of bioactivities, including antibacterial, antiviral, and anti-inflammatory properties. Of particular interest is its potential for anticancer activity on gastric cancer cell lines, which has been supported by fairly numerous research studies [6]. The compounds in propolis have unique phytochemical compositions, such as flavonoids, phenolics, and other bioactive molecules, which contribute to their ability to inhibit tumor growth and induce apoptosis in cancer cells [7]. For example, quercetin shows effective cytotoxicity against a human gastric adenocarcinoma cell line (AGS cells) with IC_{50} values of 160 μM by inducing apoptosis via mitochondrial pathways [8]. Additionally, pinocembrin (purified compound from New Zealand propolis) has been shown to be effective against NCI-N87 gastric cancer cells, with a 72.5 % cytotoxic activity at 200 μg/mL [9]. Each of these compounds has distinct mechanisms of action, making them compelling subjects for further gastric cancer research. Additionally, the cytotoxic activity of crude propolis extracts from various regions in Thailand against gastric cancer cell lines (KATO-III) exhibited varying IC_{50} values, ranging from 14.50 to 35.55 μg/mL, depending on the source of propolis from each region [10]. Thus, recognizing the chemical makeup of propolis, which varies based on several factors, including the plants the bees collected from, geographic location, seasonal variations, and even the specific bee species involved [11], is critical. Significant differences in the composition and biological properties of propolis can be found within a country and in different regions. For example, southern green propolis in Brazil may contain more artepillin C, which has anti-inflammatory and antitumor properties. In contrast, northeastern red propolis may contain more formononetin, which has antioxidative properties [12]. These regional variations occur due to the interaction of the local flora and bee species, thereby emphasizing the relevance of considering regional factors in the study of propolis. Understanding the influence of these factors is crucial for elucidating the diverse therapeutic potentials of propolis and informing targeted research efforts.

In Thailand, Ratchaburi is a province with a diverse range of plant species, influenced by its geography and climate. Indeed, one district called Suan Pueng can be translated as Bee Garden, which implies a region abundant with nature, where bees might thrive [13]. Ratchaburi is characterized by tropical seasonal forests, deciduous forests, and mixed deciduous forests. The region's proximity to mountainous areas and its varied topography likely contribute to the diverse vegetation types. The dominant tree species include *Thysostachys siamensis*, with an average abundance of 15,342 individuals/hectare [14], while other species, such as *Anisoptera costata* and *Areca catechu* L., are also prevalent in different areas of Ratchaburi [15].

As mentioned earlier, bee species are a factor involved in the diverse array of specific compounds in propolis that are responsible for bioactivites. *Tetragonula laeviceps* is a stingless bee species distributed in Southeast Asia, including Thailand. This species was selected for study based on its prevalence as the leading stingless bee species across all of Thailand [16]. Moreover, this native stingless bee species can produce relatively large amounts of propolis. Researchers have been increasingly drawn to the bioactivities of propolis from stingless bee species, due to its unique chemical composition distinct from the propolis of other bee species. The propolis of *T. laeviceps* from Samut Songkram province was shown to have cytotoxic activites against the KATO-III cell line, with an IC_{50} of 4.09 μg/mL [17]. Also, gamma- and alpha-mangostin purified from the propolis of *Tetragonula pagdeni*, *Lepidotrigona ventralis*, and *Lepidotrigona terminata* in Thailand's Chantaburi province inhibited the migration of several cancer cells, including colorectal cancer (Caco-2), papilloma carcinoma (KB), melanoma (SK-MEL-28), and head, neck (HN30) cancer cells [18]. A study conducted in Thailand highlighted varied anticancer effects of propolis, with the observed variations depending on its geographic source. However, there are areas rich in bees that lack information on the bioactivity of their respective propolis, preventing a further understanding of the significance of geographical variations in propolis and its therapeutic potential.

This research seeks to fill gaps in knowledge regarding the bioactivity of propolis from areas abundant in bees. This study aims to deepen our understanding of the implications of geographical variations in propolis and its therapeutic potential by identifying and characterizing bioactive compounds from the propolis of *T. laeviceps* whose hives were amongst native plants in the Bankha district, Ratchaburi, Thailand. Additionally, the cytotoxic effects of these compounds on both KATO-III gastric cancer cell lines and WI-38 normal fibroblast cell lines are sought to be investigated using the 3-(4,5-dimethylthiazol-2-yl)-2,5-diphenyltetrazolium bromide (MTT) assay. The research involves isolating and fractionating the bioactive compounds, assessing their cytotoxicity, investigating their impact on cellular morphology, analyzing programmed cell death and cell cycle arrest, and evaluating alterations in gene expression associated with cancer progression. Overall, the acquired results offer a more comprehensive perspective on the inhibitory effects of the purified compound on the growth of KATO-III gastric cancer cells.

2. Material and methods

2.1. Propolis collection, extraction, and partition

Propolis from the stingless bee, *Tetragonula laeviceps*, was collected from a specific site in Bankha district, Ratchaburi province, Thailand (13°22′03.2″ N, 99°25′12.5″ E). The plant species in the vicinity of the sampling areas are listed in Table 1. The extraction and partition procedures were performed as previously reported, starting with an initial 80.27 g of propolis [19]. Following that, the crude hexane, dichloromethane (DCM), and MeOH partitioned extracts (HPE, DPE, and MPE, respectively) were obtained and examined for their cytotoxic properties.

2.2. Further enrichment of the active crude extract

The most cytotoxic extract against the KATO-III cell line was further fractionated to identify the pure compound(s) responsible for the cytotoxic activity. The fractionation process was carried out concurrently with bioactivity testing as previously reported [10]. A schematic illustration of the propolis screening and enrichment process for evaluating cytotoxic activities in the most potent extract is presented in Fig. 1.

2.2.1. Fractination by SiG60-CC and SSECC

2.2.1.1. Large scale SiG60-CC (500-mL column). The most active partitioned extract was further fractionated by SiG60-CC using a 500-mL column. The DPE (1.95 g) was dissolved in 30 mL of DCM and mixed with 30 g of rough SiG60 (Merck, for CC). The DPE-SiG60 mixture was left to dry and then poured onto the packed column. The column was then eluted with a mobile phase of 5 L of 1: 1 (v/v) ethyl acetate (EtOAc): hexane followed by 2 L of 3:1 (v/v) EtOAc: hexane and 2 L of EtOAc, collecting 50 mL fractions. The pattern of chemical compounds in each fraction was determined by TLC. Those fractions with a similar TLC pattern were pooled and then screened for cytotoxic activity using the MTT assay. The active pooled fractions from the large-scale process were then further enriched by small scale (250-mL column) SSECC and SG60-CC.

2.2.1.2. Small scale SSECC. Sephadex LH-20 gel (120 g, GE Health care Bio-sciences AB) was swollen in absolute MeOH (500 mL) for 2 h before loading the fractions in the 250-mL column. The obtained active fraction (F2; pooled from fractions 19–29) was dissolved in DCM and then loaded on the column and eluted with 400 mL of 3: 2 (v/v) DCM: EtOAc followed by 200 mL of 4: 1 (v/v) DCM: EtOAc and 100 mL of DCM, collecting 5 mL fractions. The resulting active fraction (F4, pooled from fractions 41–62) was dissolved in DCM, transferred to the column, and eluted with 600 mL of 2 % (v/v) MeOH in DCM, collecting 2 mL fractions. Fractions were screened for component composition by TLC profile patterns, with those with similar TLC profiles being pooled. The group of fractions that showed distinct spots in the TLC system were assumed to be crucial compounds responsible for cytotoxic activity, based upon the previous observation that the majority of compounds detected in the TLC system corresponded with the bioactivity [10]. Any major spots that showed a single spot on the TLC plate were then analyzed for their chemical structure by NMR (see section 2.3). After mixing similar profiled major spots they were then further enriched using small scale SiG60-CC.

2.2.1.3. Small scale SiG60-CC (250-mL column). As described above, 250-mL SG60-CC in DCM was prepared. The selected SSECC

Table 1
The different plant species within a 500-m radius around the *T. laeviceps* hives in Bankha, Ratchaburi province, Thailand.

| Scientific name	Common name
Dipterocarpus alatus	*The resin tree, yang na*
Coffea arabica	*Coffee plant*
Artocarpus heterophyllus	*Jack fruit*
Maerua siamensis	*Chaeng*
Phyllanthus acidus	*Tahitian gooseberry tree*
Casuarina junghuhniana	Horsetail tree
Cocos nucifera	*Coconut tree*
Dendrocalamus latiflorus	*Sweet bamboo*
Xanthostemon chrysanthus	*Golden penda*
Areca catechu	*Betel palm*
Flacourtia indica	*Ramontchi*
Zollingeria dongnaiensis	*Kee non*
Mangifera indica	*Mango*
Typha angustifolia	*Cat-tail*
Fallopia japonica	*Japanese knotweed*
Dalbergia cochinchinensis	*Siamese rosewood*
Ananas comosus	*Pineapple*
Saccharum officinarum	*Sugarcane*
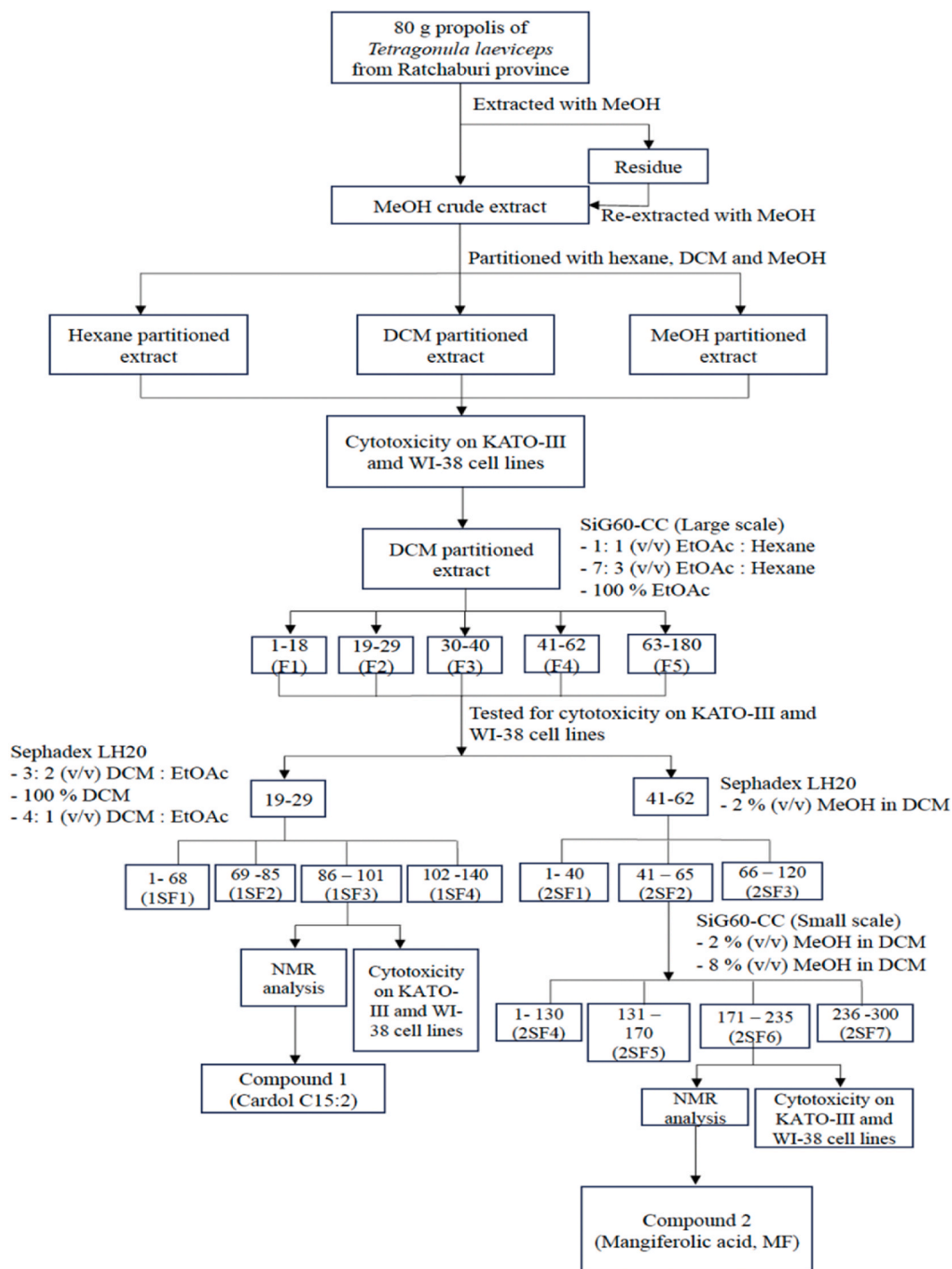
Fig. 1. Extraction and isolation scheme of selected extracts.

fraction for further enrichment was dissolved in 2–8 % (v/v) MeOH in DCM, combined with SG60 (5–10 g), and left until dry. The silica-coated fraction was gradually poured over the top surface of the SG60 column and then eluted with a mobile phase of MeOH and DCM ranging from 0: 100 to 10: 90 (v/v) MeOH: DCM, collecting 5 mL fractions. Fractions with similar chemical profiles on the TLC plate were pooled together and assessed for cytotoxic activity using the MTT assay.

2.2.1.4. Comparative component analysis by TLC. A 5 × 5 cm^2 TLC plate with silica as the immobile phase was prepared. The samples

from section 2.2.1 were spotted onto the starting line using a capillary tube and dried at room temperature. The TLC plates were placed in a small glass chamber and then developed in one direction using the same mobile phase applied in the column (section 2.2.1). After the mobile phase reached the solvent front, the TLC plate was removed, left at room temperature to dry, and then visualized under UV light at 254 nm followed by dipping in 3 % (v/v) anisaldehyde in MeOH and heating over a hot plate. Fractions displaying the same pattern of chemical compounds were pooled and tested for cytotoxic activity against cancer cell lines.

2.3. Chemical structure analysis by ^1H and ^{13}C NMR

The bioactive compounds enriched to potential purity were characterized by NMR spectroscopy [20]. Briefly, the active fractions were evaporated and dissolved in deuterated chloroform ($CDCl_3$) at a ratio of 5–7 mg of compound to 600 μL of deuterated solvent, transferred to an NMR tube and shaken until homogeneous. The ^1H NMR and ^{13}C NMR spectrums were recorded using a JEOL JNM-ECZ500R/S1 500 MHz NMR spectrometer machine operating at 500 and 256 MHz for ^1H and ^{13}C NMR nuclei, respectively, with tetramethylsilane as the internal standard. The chemical shift value in δ (ppm) was assigned regarding the signal or the residual protons in the deuterated solvents. Chemical shifts and J coupling values are reported in ppm and Hz using MestReNova version 12.0.3 software.

2.4. Cell culture and cell lines

The gastric carcinoma or stomach cancer (KATOIII-HTB103/ATCC) cell line was utilized in the study to assess the *In Vitro* anti-proliferative activity. The KATO-III cell line was cultured in RPMI 1640 media (Invitrogen) supplemented with 10 % (v/v) fetal bovine serum (FCS; Gibco). Additionally, the untransformed (normal) lung fibroblast line WI-38 (ATCC No. CCL-75) was employed as a reference to assess the selective specificity of the treatment towards cancer cells rather than all cells that divide. The normal cell line was cultured in Eagle's Minimum Essential Medium containing 10 % (v/v) FCS. The two cell lines were cultured and tested at 37 °C, with a carbon dioxide (CO_2) concentration of 5 % (v/v) in a humidified environment.

2.5. Cell viability determination using the MTT assay

The cytotoxic activity against the KATO-III cell line of the partitioned extract and active fractions during the purification process was conducted as previously reported [21]. The KATO-III cell line was seeded at 1×10^4 cells per well in a 96-well plate. Each well contained 198 μL of complete media. The plate was then cultured under the same conditions described above for 24 h to allow the cells to adhere to the bottom of each well. At the same time, WI-38 cells were adjusted with complete media to 1×10^5 cells/well in a 96-well plate containing 198 μL of medium and incubated overnight. Subsequently, the KATO-III and WI-38 cells were treated with various concentrations of the partitioned extract or active fractions (2 μL per well) dissolved in dimethylsulfoxide (DMSO) [22]. The positive control in this study involved the use of doxorubicin (Sigma-Aldrich, St. Louis, MO) at different concentrations. The negative control group was determined by adding 2 μL DMSO to each well without additional substances, resulting in a 1 % (v/v) DMSO concentration. All cell lines were further incubated for 24, 48, and 72 h. After the specified period, 10 μL of 5 mg/mL MTT (Sigma-Aldrich, St. Louis, MO) solution in phosphate buffer saline (PBS) was added into each well and incubated for another 4 h to allow formazan formation. The supernatant was removed, and 150 μL of DMSO was added to each well to dissolve the formazan crystals. The absorbance measurement was conducted at a wavelength of 540 nm (A_{540}). The percentage of viable cells relative to control was calculated as follows:

$$\text{The relative (\%) number of viable cells} = \frac{\text{(Abs of sample) x 100}}{\text{Abs of control}}$$

The IC_{50} value (in microgram per millilitre) of each treatment was calculated from the plot of test sample concentration (X axis) against the relative cell viability percentage (Y axis). Three replications of each trial were performed.

2.6. Programmed cell death

The test cells were cultured as described in section 2.4. The KATO-III cells were seeded at 5×10^5 cells per well into 6-well plates, cultured overnight, and then treated the following day with (i) the test compound dissolved in DMSO at final concentration of 0, 7.5, 15, and 30 μg/mL, (ii) doxorubicin (1.14 μg/mL), and (iii) 1 % (v/v) DMSO only as a control. After 24, 48, and 72 h of incubation at 37 °C with 5 % (v/v) CO_2, the treated cells were harvested by trypsinization with 0.05 % (w/v) trypsin in 0.05 mM in ethylenediaminetetraacetic acid buffer, washed twice with cold phosphate-buffered saline (PBS) using centrifugation at 3,000×g for 5 min to harvest the cells each time. The washed cell pellets were then resuspended in 100 μL of 1× binding buffer (10 mM HEPES, pH 7.4, 140 mM NaCl, and 2.5 mM $CaCl_2$) and stained with 5 μL annexin V (catalog. A13201, Thermo Fisher Scientific Inc., MA, USA) for 15 min at room temperature (RT) in the dark. Cells were then washed twice with PBS as above, resuspended in 100 μL of binding buffer, and then stained with 5 μL of 1 mg/mL propidium iodide (PI) solution at RT in the dark for 15 min on ice. The samples were then analyzed using flow cytometry (Beckman Coulter, Brea, CA). The experiment was performed in triplicate.

2.7. Cell cycle arrest analysis

To determine the phase distribution of DNA content, KATO-III cells were cultured in complete media and seeded at 5×10^5 cells per well into 6-well plates. Cells were treated with purified compound at a final concentration of 0, 7.5, 15, and 30 µg/mL for 24, 48, and 72 h at 37 °C with 5 % (v/v) CO$_2$. As a negative control, 1 % (v/v) DMSO alone was added to the cells. After incubation (24–72 h), the treated cells were harvested as outlined for the apoptosis detection in section 2.6 and fixed in 400 µL of 70 % (v/v) ethanol on ice for 30 min. Fixed cells were then washed twice with PBS as before except at 4 °C for 5 min. Then, the cell pellet was resuspended in 200 µL of PBS containing 100 µg/mL RNase A and incubated for 30 min at 37 °C. Next, the cells were washed as described above, resuspended, and stained with 300 µL of 50 µg/mL PI in PBS and incubated at 37 °C for 30 min at RT. Flow cytometric analysis was then performed on a FC 500 MPL cytometer (Beckman Coulter, Brea, CA) recording 10,000 events per sample. The experiment was performed in triplicate.

2.8. Cell imaging

KATO-III cells were seeded at a density of 5×10^5 cells per well in 6-well plates. After 16 h of incubation, the cells were then treated with 1 % (v/v) DMSO as a negative control, or with doxorubicin (1.14 µg/mL), or with purified compound (7.5, 15, and 30 µg/mL) for 24, 48, and 72 h. Morphological changes were observed using Nikon Eclipse TS100 microscope coupled with a DS-L3 imaging system at $100\times$, and $200\times$ magnifications.

2.9. Evaluation of the expression levels of selected cancer-associated genes by RT-qPCR

The cell lines were cultured and treated as outlined for the apoptosis detection in section 2.6. After treatment, the cells were harvested using a cell scrapper, Adherent and floating cells were collected and washed twice with cold phosphate-buffered saline (PBS) using centrifugation at $3,000\times g$ for 5 min to harvest the cells each time. Then, the total RNA was extracted using an RNeasy mini kit (Catalog No. 74104; Qiagen, Valencia, CA, USA). The quantity and integrity of RNA were spectrophotometrically evaluated as an A_{260}/A_{280} nm ratio. Three groups of treated cells were prepared: 1 % (v/v) DMSO alone (negative control), 1.14 µg/mL doxorubicin (positive control), and purified compound **2** (30 µg/mL). The samples were kept at -80 °C until used to evaluate the transcript expression levels of the inflammation-associated genes (*COX2* and *NFkB*), proto-oncogene (*CTNNB1*), autophagy-associated gene (*CTSB*), and apoptosis-associated genes (*BCL-2*, *CASP3*, and *CASP7*). The RT-qPCR was conducted using the One-Step TB Green® PrimeScript™ RT-PCR Kit II (Perfect real time; catalog No. RR086A, Takara, Japan), following the manufacturer's instructions. Each reaction was performed in a final volume of 10 µL, including of 15 ng of total RNA, 0.5 µL of PrimeScript™ Enzyme Mix II, $1\times$ One-Step TB Green® RT-PCR Buffer IV, and 0.5 µL of each forward and reverse primer (10 µM). The primer sequences were derived from previous studies [21] and are shown in Table 2. Glyceraldehyde-3-phosphate dehydrogenase (*GAPDH*) was used as the endogenous expression standard. The relative expression levels of target genes were normalized to the expression level of the *GAPDH* as a control. Each RT-qPCR assay was performed in triplicate using a thermal cycling program of 95 °C for 10s, followed by 40 cycles of 95 °C for 10 s and 60 °C for 30s.

2.10. Statistical analysis

All data are presented as the mean ± standard deviation (SD). Statistical analysis of the data was performed using one-way analysis of variance (ANOVA) followed by Tukey's multiple comparisons test for the significance of differences between the means. Data was considered statistically significant at the $P < 0.05$ and $P < 0.01$ levels.

Table 2
Targeted genes and primer sequences [19].

Gene	Forward primer (5' → 3')	Reverse primer (5' → 3')
Reference gene		
GADPH	GGGCATCCTGGGCTACTCTG	GAGGTCCACCACCCTGTTGC
Apoptosis-associated genes		
BCL-2	ATGTGTGTGGAGACCGTCAA	GCCGTACAGTTCCACAAAGG
CASP3	TGTTTGTGTGCTTCTGAGCC	CACGCCATGTCATCATCAAC
CASP7	CCAATAAAGGATTTGACAGCC	GCATCTGTGTCATTGATGGG
Inflammation-associated genes		
COX2	TCTGCAGAGTTGGAAGCACTCTA	GCCGAGGCTTTTCTACCAGAA
NFkB	ATGGCTTCTATGAGGCTGAG	GTTGTTGTTGGTCTGGATGC
Proto-oncogene		
CTNNB1	CTTGTGCGTACTGTCCTTCG	AGTGGGATGGTGGGTGTAAG
Autophagy-associated gene		
CathepsinB	CAGCGTCTCCAATAGCGA	AGCCCAGGATGCGGAT

3. Results

The bioactive composition of propolis is greatly influenced by the origin of resin nearby. The prevalent species of plants surrounding the sampling site in Bankha district, Ratchaburi province are shown in Table 1.

The characteristics of each crude extract (yield, weight, and appearance) were previously reported, including those of the HPE (4.80 %, 3.86 g, and light brown oil), DPE (2.43 %, 1.95 g, and sticky brown liquid), and MPE (12.29 %, 9.87 g, dark brown liquid) [19], while preliminary screening for *In Vitro* cytotoxic activity against the KATO-III and WI-38 cell lines at a single concentration of 100 µg/mL showed that the DPE was the most cytotoxic of the three partitioned extracts [10] with an IC_{50} value against the KATO-III cancer cells and WI-38 control cell lines after 48 h treatment of 35.15 ± 1.69 and 46.52 ± 0.31 µg/mL, respectively. Thus, here the DPE was subjected to further enrichment due to its higher cytotoxicity to cancer cells than normal cells, although it was not as effective as doxorubicin.

3.1. Cytotoxic effect of the enriched fractions on the KATO-III cell line

Since the DPE presented the best selective antiproliferative activity against the KATO-III cancer cell line of the three crude extracts, as determined by comparison of the IC_{50} values, it was selected for further partial enrichment by quick column SG60-CC. Five fraction groups (F1–5) were obtained from the different elution solvent mixtures with two major components being found in fractions F2 and F4 at a 28.71 % and 25.12 % yield, respectively, (Table 3). Fractions F1, F3, and F5 were minor components with a light-smear band visible on the TLC profiles patterns. Fractions F1–5 were determined for their cytotoxicity against the two cell lines after 48 h. Of the five fractions, fraction F2 exhibited the highest cytotoxic activity against the two selected cell lines, with IC_{50} values ranging from 9.048 ± 0.792 µg/mL for KATO-III to 13.778 ± 0.145 µg/mL for WI-38. In addition, fraction F4 also provided a high cytotoxic activity with IC_{50} values ranging from 11.882 ± 0.662 µg/mL for KATO-III to 14.800 ± 0.062 µg/mL for WI-38. In contrast, no significant activity (IC_{50} values > 50 µg/mL) was detected in fractions F1, F3, and F5 (Table 3).

Since DPE fractions F2 and F4 exhibited the highest cytotoxic activities against the KATO-III cell line, these fractions were further enriched by SSE-CC. For fraction F2, four sub-fractions (yielding 140 fractions) were obtained with varying appearances (Table 3). In the sub-fraction groups, the dominant spot was clearly observed in sub-fractions 86–101 (1SF3) with a major orange solid spot (Fig. 2). This apparently pure spot found in fraction 1SF3 was designated compound **1** and assumed to be responsible for the cytotoxic activity in that fraction because the other non-active subfractions in fraction F2 showed an almost undetectable or faint spot. At the same time, the clear dark blue spot was detected in the TLC pattern profiles of fraction F4 in sub-fractions 41–65 (2SF2) mixed with minor components after SSECC. The sub-fraction 41–65 (2SF2) of fraction F4 was then further enriched by SiG60-CC (250-mL) to yield a total of 300 fractions. After pooling fractions with a similar TLC profile, only the dark blue sharp band was observed in sub-fraction 171–235 (2SF6), which appeared homogeneous and was labelled as compound **2**. Compounds **1** and **2** were both found to have a strong cytotoxic activity against the KATO-III cell line with the derived IC_{50} values against the KATO-III and WI-38 cell lines reported in Table 3. Compound **1** had a 1.15- to 1.20-fold lower IC_{50} value against KATO-III cells than against WI-38 at 24, 48, and 72 h (Table 3). Compound **2** also had a 1.13- to 2.24-fold lower IC_{50} value against the KATO-III cell line than the WI-38 cell line at 24, 48, and 72 h. Although compounds **1** and **2** showed a high cytotoxicity to the normal WI-38 cell line, it was still less than that against the KATO-III cancer cell line, indicating its potentially effectiveness for application. However, these two compounds exhibited lower inhibitory effects compared to doxorubicin, which demonstrated more than a 5-fold higher cytotoxicity against both cancer and normal cell lines

Table 3
Characteristics and cytotoxic activities against the KATO-III and WI-38 cell lines of the different pooled fractions of DPE after SIG60-CC and SSECC. Data are shown as the mean ± SD derived from three repeats.

| Fraction	Weight (g)	Yield (%)	Appearance	IC_{50} (µg/mL) on KATO-III at 48 h	IC_{50} (µg/mL) on WI-38 at 48 h
After SG60-CC (Large scale):					
1–18 (F1)	0.11	5.64	Light brown oil	>50	>50
19–29 (F2)	0.56	28.71	Sticky red brown solid	9.04 ± 0.79	13.78 ± 0.14
30–40 (F3)	0.07	3.58	Pale brown solid	>50	>50
41–62 (F4)	0.49	25.12	Light brown solid	11.89 ± 0.62	14.80 ± 0.06
63–180 (F5)	0.28	14.35	Sticky brown solid	>50	>50
Fraction	**Weight (g)**	**Yield (%)**	**Appearance**	**IC_{50} (µg/mL) on KATO-III**	**IC_{50} (µg/mL) on WI-38**
After SSE-CC of pooled fraction 19–29:					
Fraction 86–101 (Compound **1**) (1SF3)	0.41	73.21	Sticky red orange solid	24 h–15.53 ± 0.53 48 h–9.73 ± 0.34 72 h–3.22 ± 0.23	24 h–18.35 ± 0.61 48 h–11.23 ± 0.45 72 h–3.89 ± 0.39
After SG60-CC (Small scale) of pooled fraction 41–62:					
Fraction 171–235 (Compound **2**) (2SF6)	0.33	67.34	Sticky light brown solid	24 h–16.02 ± 0.62 48 h–11.98 ± 1.29 72 h–4.78 ± 0.59	24 h–22.04 ± 0.48 48 h–13.65 ± 0.62 72 h–11.61 ± 1.82
Doxorubicin	–	–	–	24 h–1.55 ± 0.04 48 h–1.43 ± 0.02 72 h–0.56 ± 0.03	24 h–0.78 ± 0.01 48 h–0.09 ± 0.02 72 h–0.02 ± 0.01
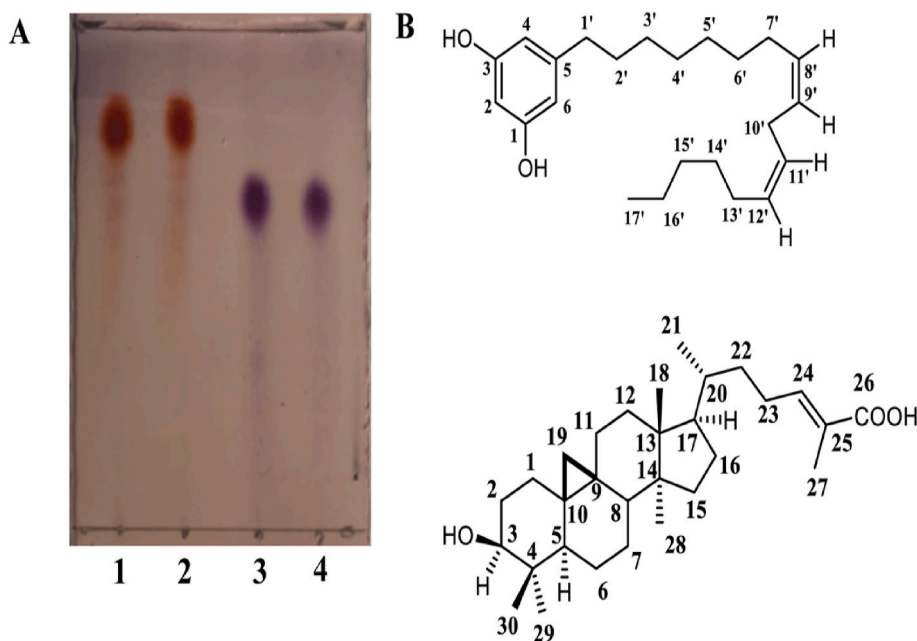
Fig. 2. (A) The TLC profiles of compound **1** (cardol C15:2, (5-[8(Z), 11(Z)-pentadecadienyl]resorcinol)) in lanes 1 and 2 and compound **2** (MF) in lanes 3 and 4 after developing in 3 % (v/v) anisaldehyde in MeOH. The mobile phase was 3:2 (v/v) DCM: EtOAc. (B) The structures of compounds **1** (cardol C15:2) (above) and **2** (mangiferolic acid, MF) (below), found in fraction 1SF3 and 2SF6, respectively.

(Table 3). The chemical structure of compounds **1** and **2** were then evaluated using ^{1}H NMR.

3.2. Structure identification of compounds 1 and 2

Compound **1** was an orange solid (Fig. 2A) and showed ^{1}H-(CDCl$_3$, 500 MHz) and ^{13}C- (CDCl$_3$, 256 MHz) NMR spectra (Fig. 3A) similar to those previously reported for cardol [22,23]. Compound **1** was isolated as a dark brown gum. The ^{1}H NMR spectrum revealed signals for aromatic and aliphatic protons. The first set, three *meta*-coupled aromatic protons at [δ_H 6.24 (2H, s, H-4 and H-6) and δ_H 6.17 (1H, s, H-2)]. The olefinic protons signal at δ_H 5.35 (4H, m, J = 7.40 Hz). The methylene protons displayed δ_H 2.78 (2H, t, J = 6.5 Hz, H-10′), δ_H 2.43 (2H, t, J = 7.40 Hz, H-1′), δ_H 2.02 (4H, m, H-7′ and H-13′) δ_H 1.52 (2H, brs, H-2′), δ_H 1.17–1.39 (20H, brs), and δ_H 0.89 (3H, t, J = 7.40 Hz). The NMR data of compound **1** displayed 22 signals indicated for aromatic six signals and seventeen signals for aliphatic. The first set, aromatic signals at C-1 and C-3 (δ_C 156.0), C-2 (δ_C 100.5), C-4 and C-6 (δ_C 108.4) and aliphatic carbons revealed seventeen signals due to one methyl, four sp^2 methine and twelve methylene at C-17′ (δ_C 14.2), C-8′ (δ_C 130.3), C-11′ (δ_C 130.0), C-9′ (δ_C 128.1), C-12′ (δ_C 128.0), C-1′ (δ_C 36.9), C-2′ (δ_C 31.2), C-3′ (δ_C 29.8), C-4′ (δ_C 29.8), C-5′ (δ_C 29.6), C-6′ (δ_C 29.6), C-7′ (δ_C 29.4), C-10′ (δ_C 25.7), C-13′ (δ_C 27.3), C-14′ (δ_C 29.6), C-15′ (δ_C 31.6), and C-16′ (δ_C 22.8). Thus, the NMR spectrum of compound **1** could identify a structure of cardol C15:2 (5-[8(Z), 11(Z)-pentadecadienyl]resorcinol) (Fig. 2B).

Mangiferolic acid (MF; compound **2**) was obtained as a white amorphous solid and as a major component (Fig. 2B). The ^{1}H NMR spectrum (CDCl$_3$, 500 MHz) displayed signals of a olefinic proton [δ_H 6.90 (1H, t, J = 8.25 Hz, H-24)] and six methyl groups [δ_H 1.80 (3H, s, H-27), δ_H 0.91 (3H, s, H-21), δ_H 0.97 (6H, s, H-18 and H-29), δ_H 0.89 (3H, s, H-28), and δ_H 0.81 (3H, s, H-30)], and displayed methine protons at δ_H 3.28 (1H, m, H-3), δ_H 1.33 (1H, m, H-5), δ_H 1.55–1.62 (1H, m, H-8), δ_H 1.55 (1H, m, H-17), and δ_H 1.28–1.32 (1H, m, H-20). The cyclopropane ring showed signals at [δ_H 0.54 (1H, d, J = 4.03 Hz, H-19), and δ_H 0.32 (1H, d, J = 4.03 Hz, H-19)]. The ^{1}H NMR spectroscopic data displayed ten angular methylene groups at δ_H 1.62 (1H, m, H-1), δ_H 1.24 (1H, m, H-1), δ_H 1.75 (1H, m, H-2), δ_H 1.52 (1H, m, H-2), δ_H 1.49 (1H, m, H-6), δ_H 0.49 (1H, m, H-6), δ_H 1.30 (1H, m, H-7), δ_H 1.13 (1H, m, H-7), δ_H 2.03 (1H, m, H-11), δ_H 1.15 (1H, m, H-11), δ_H 1.61 (2H, m, H-12), δ_H 1.28–1.32 (2H, m, H-15), δ_H 1.90 (1H, m, H-16), δ_H 1.27 (1H, m, H-16), δ_H 1.55 (1H, m, H-22), δ_H 1.16 (1H, m, H-22), and δ_H 2.25 (1H, m, H-23), δ_H 2.10 (1H, m, H-22) (Fig. 3B).

The ^{13}C NMR spectrum (CDCl$_3$, 256 MHz) demonstrated 30 signals with six methyl carbons at C-18 (δ_C 18.4), C-21 (δ_C 19.7), C-27 (δ_C 12.3), C-28 (δ_C 19.7), C-29 (δ_C 25.8), and C-30 (δ_C 14.4); two olefinic carbons at C-24 (δ_C 146.2) and C-25 (δ_C 127.1); and a carbonyl carbon at C-26 (δ_C 173.8) including a cyclopropane ring at C-19 (δ_C 30.3). The ^{13}C NMR spectroscopic data also displayed eleven signals of secondary carbon astoms at C-1 (δ_C 32.3), C-2 (δ_C 30.7), C-3 (δ_C 79.2), C-6 (δ_C 21.5), C-7 (δ_C 2.3), C-11 (δ_C 26.4), C-12 (δ_C 33.2), C-15 (δ_C 35.1), C-16 (δ_C 28.5), C-22 (δ_C 35.1), and C-23 (δ_C 25.8). Three tertiary carbon signals were observed at C-5 (δ_C 47.4), C-8 (δ_C 47.7), and C-17 (δ_C 52.2) including four quaternary carbons at C-4 (δ_C 40.8), C-9 (δ_C 19.7), C-10 (δ_C 26.4), C-13 (δ_C 45.7), and C-14 (δ_C 48.3) (Fig. 3B).

After enrichment to apparent homogeneity both compounds **1** and **2** demonstrated a cytotoxic potential, but this study primarily concentrated on compound **2** (MF), due to its lesser-known bioactivity in the scientific field, particularly in relation to its cytotoxic
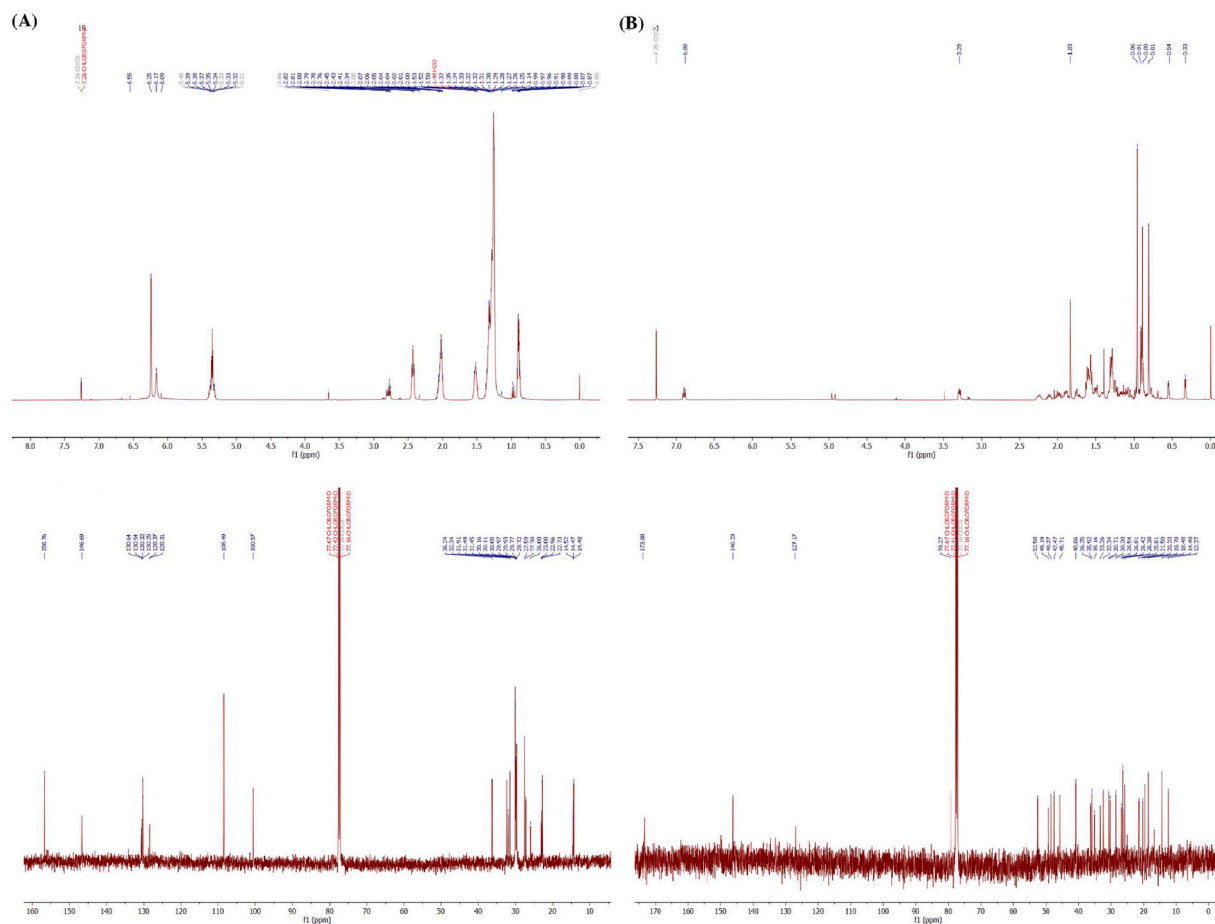
Fig. 3. (A) ^{1}H- (500 MHz in CDCl$_3$) (above) and ^{13}C- (CDCl$_3$, 256 MHz) (below) NMR spectra of compound **1** (cardol C15:2 (5-[8(Z), 11(Z)-penta-decadienyl]resorcinol)) (B) ^{1}H- (500 MHz in CDCl$_3$) (above) and ^{13}C- (CDCl$_3$, 256 MHz) (below) NMR spectra of compound **2** (Mangiferolic acid, MF).

effects on the KATO-III cancer cell line. While compound **1** (cardol C15: 2) was also identified and characterized, it is well-established as a natural bioactive product [22].

3.3. Morphology of KATO-III cells after in vitro exposure to compound 2 (MF)

After 24, 48, and 72 h treatment of KATO-III with 15 and 30 µg/mL of MF, the changes in the morphology of the treated cells (1 % DMSO) were observed (Fig. 4).

The shape of KATO-III cells under the control condition (DMSO) at all time points mainly appeared in three forms: adherent cells, non-adherent cells, and spheroid cell clusters (Fig. 4B), confluently spread over the wells. Treatment with MF directly affected the density and the number of cells in a dose-dependent manner. However, the lowest evaluated concentration (7.5 µg/mL) was not effective in large-scale cultures (5×10^5 cells in 2 mL of medium in 6 well plates), where KATO-III cells treated at this concentration at all time points seemed similar to the control cells. On the other hand, when increasing the concentration four-fold to 30 µg/mL (the average IC$_{50}$ value), obvious changes were detected after 48 and 72 h of treatment. At $100\times$ magnification, a lower density of cells was noted at 48 h and this was even more drastically reduced after 72 h of treatment at 30 µg/mL. Moreover, the treated cells at this concentration had a higher proportion of round cells, cell shrinkage, and cell debris (Fig. 4B). No significant change in the morphology of cells treated with MF at 15 µg/mL at 24 and 48 h were detected except for the reduction in the adherent cell density and cell size compared to the control (Fig. 4B). For comparison, treatment with doxorubicin at 1.14 µg/mL resulted in cell shrinkage and blebbing after 48 h with a clear loss of cell density at 72 h (Fig. 4B). In addition, the doxorubicin-treated KATO-III cells had more vacuoles than the control cells.

3.4. Apoptosis and cell cycle arrest

Further investigation was conducted to explore the potential induction of programmed cell death (apoptosis) or necrosis, as
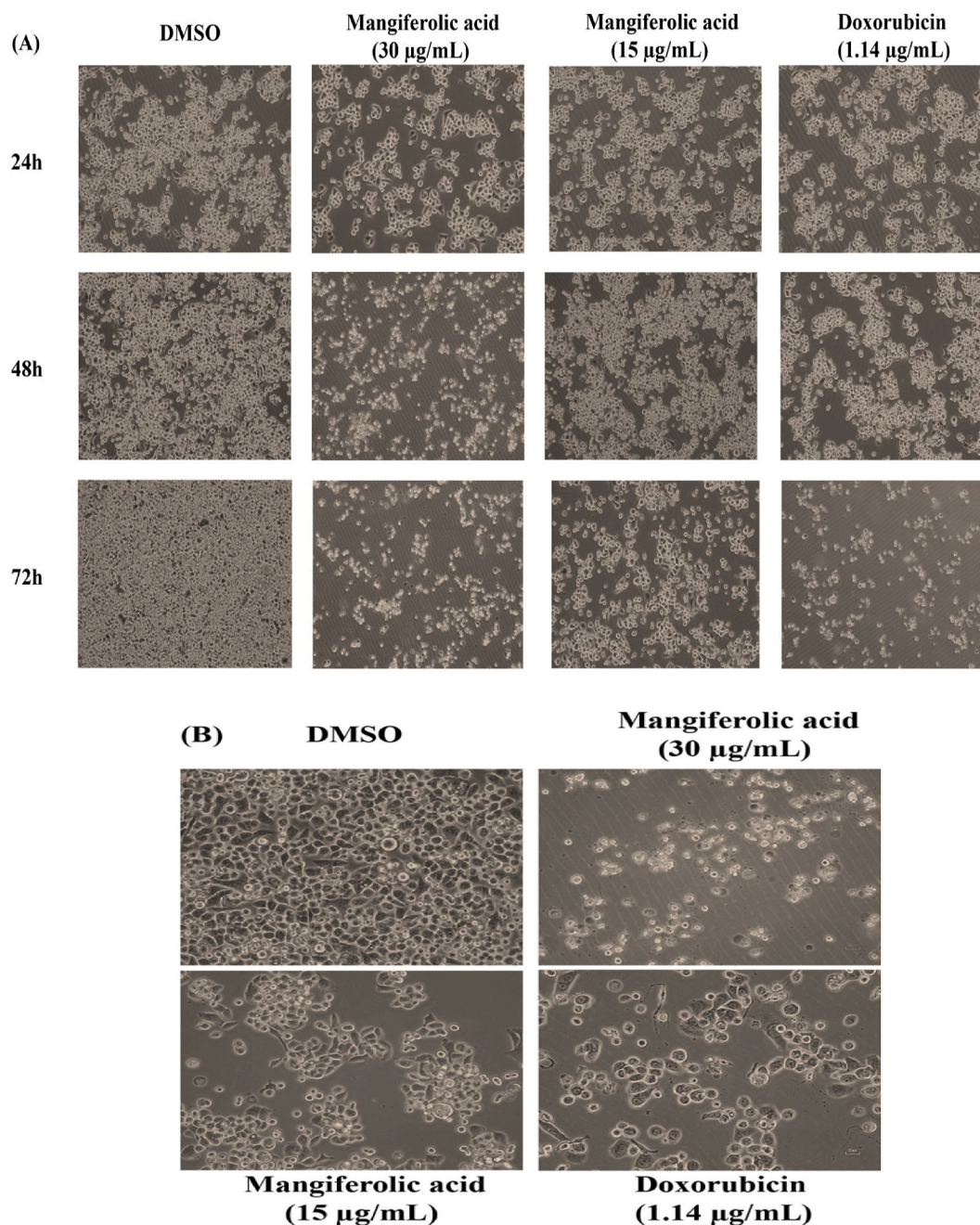
Fig. 4. Morphology of KATO-III cells treated with 1 % (v/v) DMSO alone or containing either MF at 15 and 30 μg/mL or doxorubicin (1.14 μg/mL) for 24, 48, and 72 h as viewed under (A) 100× magnification and (B) 200× magnification. Images are indicative of observations made across a minimum of three different fields of view for each sample, with the experiment conducted three separate times.

evidenced by the decreased cell density following prolonged exposure to MF or doxorubicin, as this could be due to cell death and/or inhibition of proliferation. For this MF was administered to KATO-III cells at concentrations of 7.5, 15, and 30 μg/mL for 24, 48, and 72 h. After treatment, cells were harvested and analyzed by flow cytometry for apoptosis, classifying the cells into the four groups of (i) viable cells (annexin V-FITC⁻ PI⁻), (ii) early apoptotic cells (annexin V-FITC⁺ PI⁻), (iii) late apoptotic cells (annexin V-FITC⁺ PI⁺), and (iv) necrotic cells (annexin V-FITC⁻ PI⁺), using unstained cells as a standard (Fig. 5A). After staining with annexin V-Alexa fluor 488 and PI, the results revealed that MF treatment at 30 μg/mL induced a significant level ($P < 0.01$) of necrosis in KATO-III cells from an early exposure time of 24 h onwards (Fig. 5B).

During a 24–72 h treatment period with 30 μg/mL of MF, the proportion of late stage apoptotic KATO-III cells (Annexin V⁺/PI⁺)

(A)

(B)
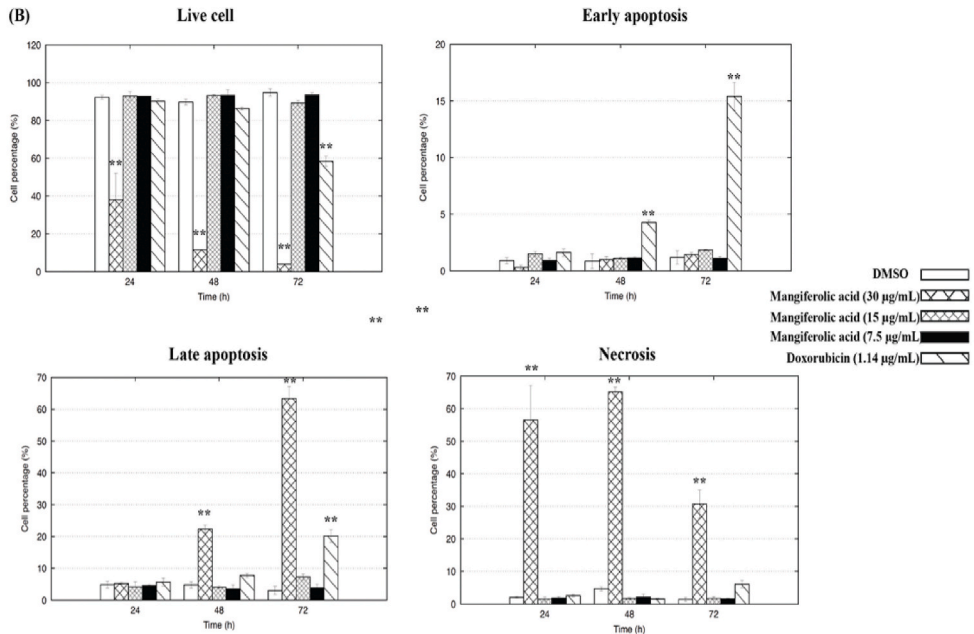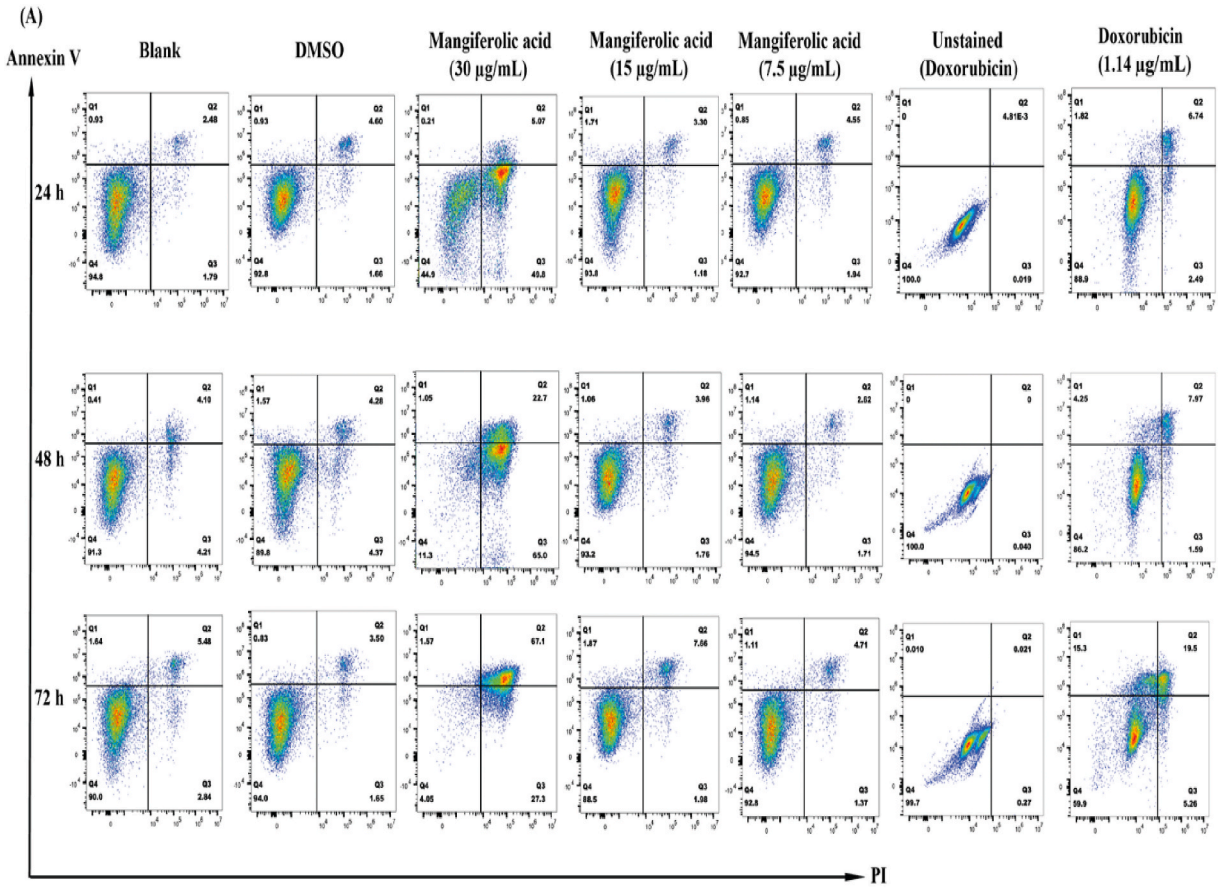
(caption on next page)

Fig. 5. Programmed cell death of KATO-III cells stained with annexin-V and PI after treatement with 1 % (v/v) DMSO alone (negative control), or containing either MF at 7.5, 15, and 30 μg/mL, or doxorubicin (1.14 μg/mL; positive control) for 24, 48, and 72 h. The (A) FACS profiles and (B) resultant histogram analysis presented in this study represent 10,000 events and are indicative of the patterns seen in three replications. The symbols "*" and "**" indicate a significant difference between the control and treated cells in each group at $P < 0.05$ and $P < 0.01$, respectively.

increased from 5.07 % to 67.1 %, showing a correlation with the duration of exposure, with the highest of late stage apoptotic cells observed at 72 h of MF treatment (Fig. 5A). While the highest average of necrosis stage cells (Annexin V$^-$/PI$^+$) was detected at 48 h of treatment (65.0 %). The incidence of necrosis in KATO-III cells induced by the 30 μg/mL MF treatment was significantly higher than in the control cells at 24 and 48 h for late apoptosis ($P < 0.01$). However, the level of apoptosis induced by 7.5 and 15 μg/mL of MF was similar to that in untreated cells at any time point except for 72 h treatment where 15 μg/mL MF showed a slightly increased level of apoptotic cells. Thus, it seems that the lower concentrations of MF (7.5 and 15 μg/mL) may not be effective for treating these cell lines. In contrast, doxorubicin (1.14 μg/mL) led to a significantly enhanced level of early apoptosis in KATO-III cells after 48 h of exposure, with longer exposure times resulting in even more early apoptotic cells. Furthermore, the level of late apoptosis induced by doxorubicin was significantly higher compared to the control ($P < 0.01$) at 72 h (Fig. 5B). Therefore, it appears that programmed cell death in KATO-III cells is triggered by MF at 30 μg/mL through various stages of apoptosis.

Subsequently, the cell cycle was examined by quantifying the cellular DNA content through flow cytometric analysis (Fig. 6A). MF at 7.5, 15 and 30 μg/mL induced detectable levels of cell cycle arrest at the sub-G1 phase and S phase population from 24 h exposure onwards ($P < 0.01$) (Fig. 6B). The highest average percentage of sub-G1 accumulation was detected at 48 h of 30 μg/mL treatment (52.40 %; Fig. 6A). Despite an increase in the average percentage of sub-G1 accumulation after 72 h of treatment with 30 μg/mL of MF, it was lower than that observed at 48 h. This suggests that MF induced cell cycle arrest during the mid phase response (48 h), consistent with the highest level of necrosis cells observed at 48 h of programmed cell death. These results indicate that MF induced DNA damage, leading to cell cycle arrest in the Sub-G1 phase and S-phase in KATO-III cells. The DNA damage at these stages may contribute to the cell entering programmed cell death, depending on the specific pathway.

3.5. Change in gene expression levels

To explore how MF might induce cell death or halt the proliferation process in KATO-III cells, the transcript expression levels of four groups of genes were evaluated and the results are summarised in Fig. 7. At 24 h of treatment with MF at 30 μg/mL, *NFkB* and *COX2* were upregulated with significant increased in *NFkB* ($P < 0.05$) (Fig. 7A). After 48 h, significant upregulation of *COX2*, *NFkB* ($P < 0.01$), *CASP3*, *CASP7*, and *CTSB* transcript levels was observed (Fig. 7B). This pattern persisted at 72 h, with all genes showing increased in gene expression compared to control cells, except for *CTSB*, which showed only a slight increase compared to control cells (Fig. 7C).

For doxorubicin, the positive control, no significant difference was detected at 24 h in these groups of genes compared to the control cells, with only a slightly increase in the expression of *CASP7*. However, from 48 h onwards, *CASP3* and *CASP7* were significantly upregulated by doxorubicin ($P < 0.05$ at 48 h; $P < 0.01$ at 72 h), with a slightly decreased (but not significant) level of *BCL-2*. Overall, MF may induce the KATO-III cells to necrosis and induce cell death by late apoptosis with a potential association with inflammation.

4. Discussion

Numerous naturally derived products can produce metabolites that are beneficial to human health. In various cases, the extraction of these chemicals is limited to plant-based sources. However, stingless bees synthesize several products that use plant resources from their environments, including propolis [24]. One of the main components isolated from propolis sourced from Ratchaburi province was compound **2**, found to be mangiferolic acid (MF). Previously, MF was shown to be the major triterpenoid that could be purified from propolis and the main propolis component came from *Mangifera indica* resin [25,26]. Based on the plants' vinicity and similar pattern of phytochemical profiles with others, the authors suggested the *M. indica* might be a possible botanical source of this propolis [27]. It is known that cardol and MF, which we purified in this study, are also present in *M. indica* resin as common components [28, 29]. It has been reported that MF isolated from the propolis of the stingless bee *Lisotrigona furua* exhibits significant cytotoxic activity against the LU-1 lung cancer and MCF-7 breast cancer cell lines with an IC$_{50}$ value of 13.33 and 62.85 μg/mL, respectively [30]. While the cytotoxic activity of MF against KATO-III gastric cell lines was observed in this study, it is noteworthy that its efficacy was comparatively lower than that of doxorubicin, suggesting differences in cellular responses and mechanisms between cancer cell types. This compound is a triterpenic acid containing a cyclopropane ring, which is usually found in bioactive fractions of propolis [31]. Cyclopropane consists of three-membered carbocyclic moieties connected to create a ring, which makes a substantial ring strain in the structure [32]. On a molecular level, the cyclopropyl group is highly electrophilic and readily reacts with amino acids and nucleotides by forming covalent adducts with DNA, resulting in DNA cleavage [33]. It is plausible to hypothesize that the presence of the cyclopropance might play a role in cell death mechanisms. However, further investigation is needed to fully elucidate the specific pathways involved and to verify its role in the observed cytotoxic effects.

Understanding how a compound's cytotoxicity is related to apoptosis and gene expression changes is crucial for designing more effective therapies or combination treatments. Multiple studies have suggested that oxidative stress, inflammation, and cancer are all closely related [34]. Inflammation can contribute to cancer development, it can also play a role in cancer cell death through immune responses, cytokines, reactive oxygen species (ROS), and activation of cell death pathways. Inflammation can result in the production
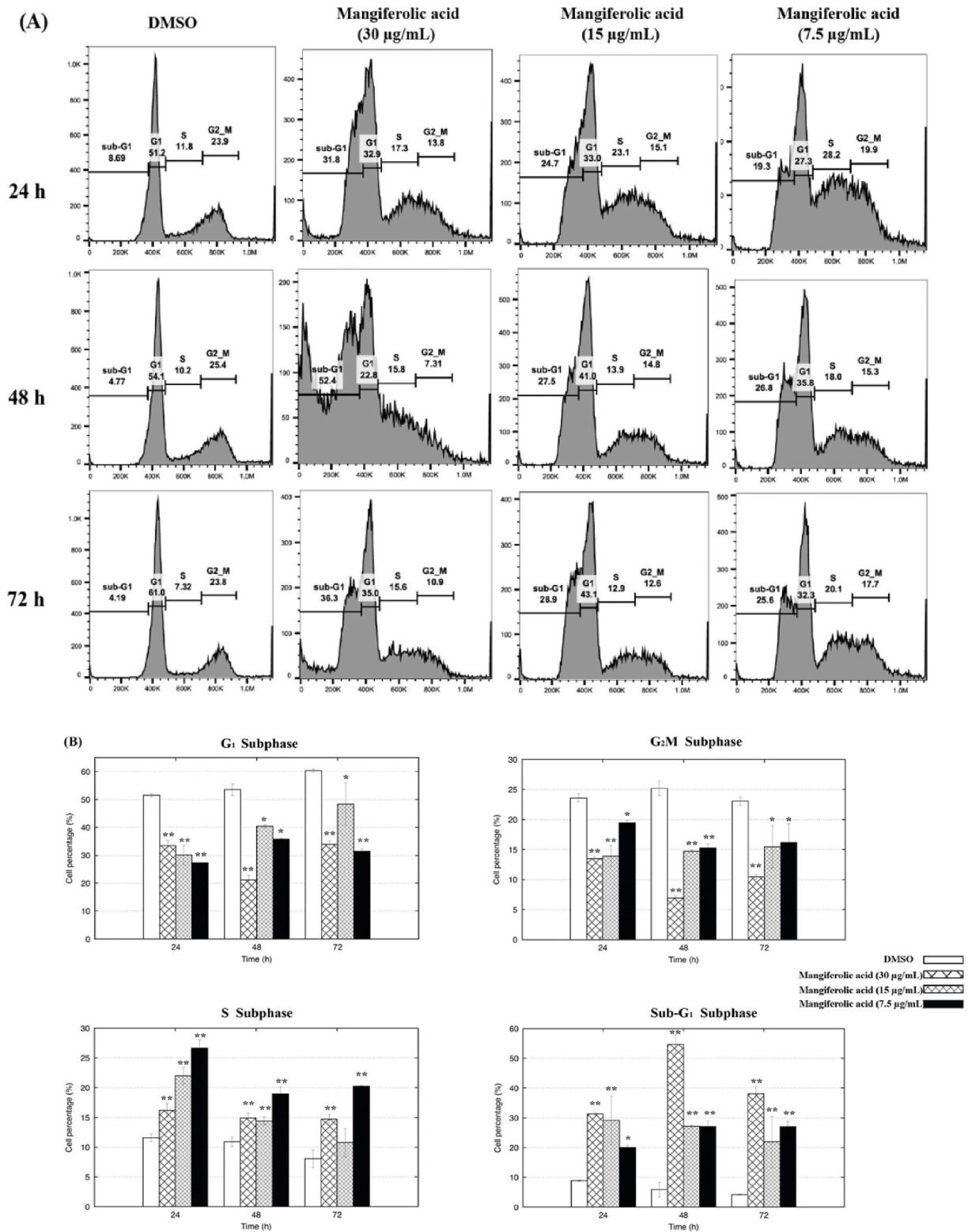
Fig. 6. Cell cycle arrest of KATO-III cells after treatment with 1 % (v/v) DMSO alone (positive control) or DMSO containing MF at 7.5, 15, and 30 μg/mL for 24, 48, and 72 h. The (A) histogram profiles (5,000 events) and (B) the percentage of KATO-III cells in each phase of the cell cycle are illustrated from three replications. The symbols "*" and "**" indicate a significant difference between the control and treated cells in each group at $P < 0.05$ and $P < 0.01$, respectively.
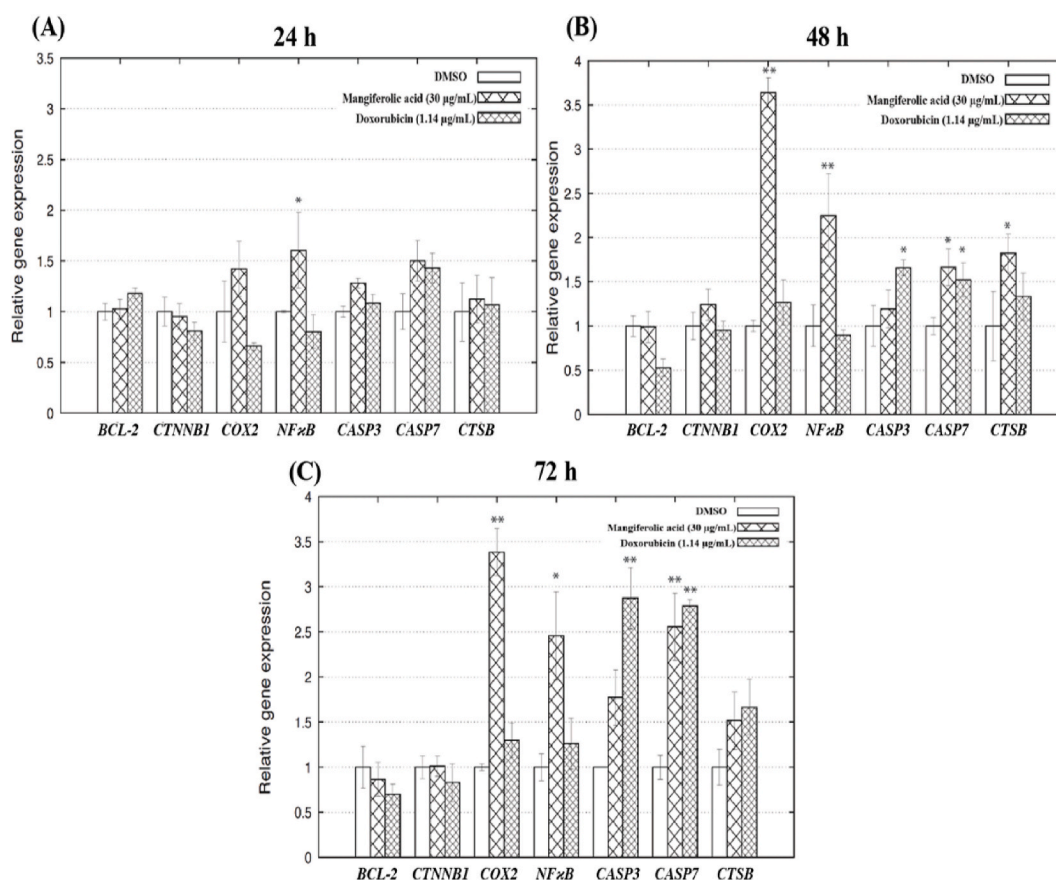
Fig. 7. Change in transcript expression levels of selected inflammation associated genes (*COX2* and *NFκB*), proto-oncogene (*CTNNB1*), autophagy associated gene (*CTSB*), and apoptosis-associated genes (*BCL-2, CASP3,* and *CASP7*). KATO-III cells were cultured for 24, 48, and 72 h with 1 % (v/v) DMSO alone or containing either MF at 30 μg/mL, or doxorubicin (1.14 μg/mL). Data are shown as the mean ± SD, derived from three independent repeats. The relative expression levels are normalized to that of the control housekeeping gene (*GAPDH*). Significant differences between the control and treated cells are shown at the P < 0.05 (*) and P < 0.01 (**) level.

of cytotoxic molecules, such as ROS. Excessive levels of ROS can damage cellular components, including DNA, proteins, and lipids [35]. Moreover, inflammation can cause immune cells to generate pro-inflammatory cytokines, such as TNF-α and interleukin-1 beta. These cytokines can trigger cell death pathways, including apoptosis in specific cell types following binding to their specific receptors that results in caspase activation and cell death [36]. In this study, MF significantly increased the transcriptional level of *NFκB* and *COX2* in KATO-III cells from the early (24 h) to late (72 h) stages of treatment. The persistence of *NFκB* and *COX2* activation may result in excessive inflammation and significant stress, or damage. This stress could lead to necrosis, especially if the treatment caused acute and severe damage to the cells. Nuclear factor-κB (*NFκB*) and *COX2* are primarily associated with regulating pro-inflammatory responses within cells, promoting the expression of pro-inflammatory cytokines [37]. Under certain conditions, *NFκB* and *COX2* activation by apigenin can also contribute to necrotic cell death in the BT-474 cell line [38]. Also, the *NFκB* signaling pathway induced *COX2* and promoted cell death in wild-type astrocytes after oxygen-glucose deprivation [39]. The activation of *NFκB* has been observed to take place during the process of cell reattachment, and this occurrence has been adapted as a potential strategy for inhibiting the survival of metastatic cells [40]. The findings were supported by the examination of programmed cell death, indicating that the treated cells died primarily by necrosis and late apoptosis (Fig. 5), which are commonly associated with inflammation [41]. Additionally, that MF induced necrosis and late apoptosis of KATO-III was supported by the observed morphological alterations (cell shrinkage, decrease in viable cell density, presence of cell debris, and round cell formation).

Flow cytometry has been used to assess the cell viability, apoptosis, and necrosis on a single cell basis. As mentioned earlier, MF induced necrosis after 24 h, indicating an earlier to late treatment response in KATO-III cells. From 48 h of treatment with MF at 30 μg/mL, late apoptosis gradually increased. Late apoptosis and necrosis are linked to inflammation, with late apoptosis potentially contributing to inflammation if not promptly cleared by phagocytosis, while necrosis triggers an immediate and uncontrolled release of cellular contents, leading to inflammation [42]. In both cases, inflammation plays a crucial role in the clearance of cell debris and tissue repair following cell death or injury. The level of late apoptosis/necrosis was increased significantly in Hep-G2 cancer cells treated with red propolis extract from Brazil, showing several biological changes of late apoptosis-like necrosis, such as membrane blebbing and shrinkage of cells to form round cells [43]. This suggests the late apoptosis and necrosis observed following MF treatment

may be mediated by inflammatory responses.

At the same time, after exposure for 48 h, the transcript levels of *CASP3* and *CASP7* were significantly upregulated, whereas that of *BCL-2* remained the same as in control cells, suggesting the increased activation of late apoptotic pathways and the execution of the orderly dismantling of the cell [44]. The transition from necrosis to late apoptosis of treated cells in this study over time may be explained by the clearance of necrotic debris and the transition to late apoptosis in the remaining cells. Macrophages and other phagotic cells in the vicinity may initially remove the cellular remnants, which is a feature of late apoptosis [45]. Also, attempts to restore cell integrity and function after necrosis involve possible repair mechanisms in response to the transition into late apoptosis to remove damaged cells [46].

An increasing proportion of cell cycle arrest at sub-G1 and S phase in the study is commonly associated with DNA degradation into small fragments, replication stress, or interference with DNA synthesis [47]. The S-phase arrest is a crucial mechanism for preventing the propagation of cells with damaged DNA. If DNA damage is detected or if conditions are unfavorable for replication (e.g., nutrient deficiency or DNA lesions), the cell cycle may be arrested at the S-phase. Also, the existence of the sub-G1 population is considered a biomarker for DNA damage, and detecting this peak signifies the occurrence of apoptosis. Submolide E compound extracted from natural products were associated to induce sub-G1 cell cycle arrest in colon cancer cells through different pathway of apoptosis [48]. In this study, *NFκB* upregulation may be part of the cellular response to DNA damage and apoptotsis, as it regulates genes involved with the processes. However, *NFκB* activation can influence the expression of the other cell cycle regulatory genes, such as cyclins and cyclin-dependent kinases, which play a role in the different phases of cell cycle.

5. Conclusion

The results demonstrate the cytotoxic potential of mangiferolic acid (MF) purified from *Tetragonula laeviceps* propolis in Ratchaburi province, Thailand. Our findings reveal that MF induces significant cytotoxicity in KATO-III cells, with an IC_{50} ranging from 4.78 to 16.02 μg/mL. Notably, the upregulation of inflammation-associated genes such as *COX2* and *NFκB* in response to the compound, along with observed changes in the cell cycle characterized by a significant rise in the sub-G1 phase and morphological alterations including decreased cell density and increased debris, are consistent with the induction of late apoptosis and necrosis, critical mechanisms in eliminating damaged cells. This research contributes to advancing our understanding of the molecular mechanisms underlying MF induced cell death in gastric cancer cells by elucidating the cytotoxic effects of MF and its impact on gene expression. These findings highlight the therapeutic potential of MF as an alternative treatment for gastric cancer, emphasizing the significance of this unique natural product. However, this study is limited to *In Vitro* experiments. Further studies using *In Vivo* models and clinical trials are necessary to validate our findings and assess the therapeutic efficacy of MF in a clinical setting. Additionally, the synergistic effect of MF with other anticancer agents needs to be elucidated to identify specific pathways involved in MF induced cell death. In the future, the efficacy of MF in gastric cancer treatment could be enhanced through application methods like fatty acid-conjugated compounds or co-administration with other promising agents for synergistic inhibition, potentially improving therapeutic outcomes.

Ethics

This work did not involve any ethical considerations or approval.

Data accessibility

Data will be made available on request.

CRediT authorship contribution statement

Thitipan Meemongkolkiat: Writing – original draft, Resources, Methodology, Formal analysis. **Songchan Puthong:** Methodology. **Phanthiwa Khongkarat:** Methodology. **Preecha Rod-im:** Methodology. **Orawan Duangphakdee:** Methodology. **Packapong Tuthaisong:** Methodology. **Preecha Phuwapraisirisan:** Writing – review & editing, Supervision, Investigation. **Chanpen Chanchao:** Writing – review & editing, Supervision, Project administration, Methodology, Investigation, Funding acquisition.

Declaration of competing interest

The authors declare that they have no known competing financial interests or personal relationships that could have appeared to influence the work reported in this paper.

Acknowledgements

References

[1] H. Sung, J. Ferlay, R.L. Siegel, M. Laversanne, I. Soerjomataram, A. Jemal, F. Bray, Global cancer statistics 2020: GLOBOCAN estimates of incidence and mortality worldwide for 36 cancers in 185 countries, Cancer J. Clin. 71 (2021) 209–249.

[2] P. Rawla, A. Barsouk, Epidemiology of gastric cancer: global trends, risk factors and prevention, Gastroenterol. Rev. 14 (2019) 26–38.

[3] W.-J. Huang, S. Ruan, F. Wen, X.-n. Lu, S.-p. Gu, X.-x. Chen, M. Liu, P. Shu, Multidrug resistance of gastric cancer: the mechanisms and Chinese medicine reversal agents, Cancer Manag. Res. 12 (2020) 12385–12394.

[4] T. Zuo, R. Zheng, H. Zeng, S. Zhang, W. Chen, Epidemiology of stomach cancer in China, Chin. Clin. Oncol. (2017) 52–58.

[5] P. Premratanachai, C. Chanchao, Review of the anticancer activities of bee products, Asian Pac. J. Trop. Biomed. 4 (2014) 337–344.

[6] E. Forma, M. Bryś, Anticancer activity of propolis and its compounds, Nutrients 13 (2021) 2594.

[7] P.B. Bhosale, S.E. Ha, P. Vetrivel, H.H. Kim, S.M. Kim, G.S. Kim, Functions of polyphenols and its anticancer properties in biomedical research: a narrative review, Transl. Cancer Res. 9 (2020) 7619–7631.

[8] H.-S. Shang, H.-F. Lu, C.-H. Lee, H.-S. Chiang, Y.-L. Chu, A. Chen, Y.-F. Lin, J.-G. Chung, Quercetin induced cell apoptosis and altered gene expression in AGS human gastric cancer cells, Environ. Toxicol. 33 (2018) 1168–1181.

[9] O. Catchpole, K. Mitchell, S. Bloor, P. Davis, A. Suddes, Anti-gastrointestinal cancer activity of cyclodextrin-encapsulated propolis, J. Funct.Foods 41 (2018) 1–8.

[10] T. Meemongkolkiat, S. Puthong, P. Khongkarat, P. Rod-im, O. Duangphakdee, P. Phuwapraisirisan, C. Chanchao, Antiproliferative and anti-tyrosinase activities of propolis from *Tetragonula laeviceps* and *Tetragonula pegdeni* in Thailand, Sains Malays. 52 (2023) 1145–1158.

[11] R. Hossain, C. Quispe, R.A. Khan, A.S.M. Saikat, P. Ray, D. Ongalbek, B. Yeskaliyeva, D. Jain, A. Smeriglio, D. Trombetta, R. Kiani, F. Kobarfard, N. Mojgani, P. Saffarian, S.A. Ayatollahi, C. Sarkar, M.T. Islam, D. Keriman, A. Uçar, M. Martorell, A. Sureda, G. Pintus, M. Butnariu, J. Sharifi-Rad, W.C. Cho, Propolis: an update on its chemistry and pharmacological applications, Chin. Med. 17 (2022) 100–160.

[12] V.C. Toreti, H.H. Sato, G.M. Pastore, Y.K. Park, Recent progress of propolis for its biological and chemical compositions and its botanical origin, Evid. Based Complement. Alternat. Med. 2013 (2013) 697390.

[13] C. Sooklim, W. Samakkarn, A. Thongmee, O. Duangphakdee, N. Soontorngun, Enhanced aroma and flavour profile of fermented *Tetragonula pagdeni* Schwarz honey by a novel yeast *T. delbrueckii* GT-ROSE1 with superior fermentability, Food Biosci. 50 (2022) 102001.

[14] U. Chaiyo, S. Garivait, K. Wanthongchai, Structure and carbon storage in aboveground biomass of mixed deciduous forest in western region, Thailand, GMSARN Int. J. 6 (2012) 143–150.

[15] U. Chanlabut, B. Nahok, Forest structure and carbon stock of Suan Phueng nature education park in Ratchaburi province, Western Thailand, Biodiversitas 23 (2022) 4314–4321.

[16] B. Chuttong, Y. Chanbang, M. Burgett, Meliponiculture: stingless bee beekeeping in Thailand, Bee World 91 (2014) 41–45.

[17] S. Umthong, P. Phuwapraisirisan, S. Puthong, C. Chanchao, *In Vitro* antiproliferative activity of partially purified *Trigona laeviceps* propolis from Thailand on human cancer cell lines, BMC Compl. Alternative Med. 11 (2011) 37.

[18] B. Vongsak, C. Chonanant, S. Machana, *In Vitro* cytotoxicity of Thai stingless bee propolis from Chanthaburi orchard, Walailak J. Sci. Technol. 14 (2017) 741–747.

[19] T. Meemongkolkiat, P. Khongkarat, P. Rodim, O. Duangphakdee, C. Chanchao, Contribution of phenolics to the antioxidant potential of propolis from *Tetragonula laeviceps* and *Tetragonula pegdeni* and its correlation to the dominant plant sources in different regions in Thailand, J. Apicult. Res. (2023) 1–10.

[20] M. Elyashberg, Identification and structure elucidation by NMR spectroscopy, Trends Anal. Chem. 69 (2015) 88–97.

[21] T. Ittiudomrak, S. Puthong, S. Roytrakul, C. Chanchao, α-Mangostin and apigenin induced cell cycle arrest and programmed cell death in SKOV-3 ovarian cancer cells, Toxicol. Res. 35 (2019) 167–179.

[22] D. Teerasripreecha, P. Phuwapraisirisan, S. Puthong, K. Kimura, M. Okuyama, H. Mori, A. Kimura, C. Chanchao, *In Vitro* antiproliferative/cytotoxic activity on cancer cell lines of a cardanol and a cardol enriched from Thai *Apis mellifera* propolis, BMC Compl. Alternative Med. 12 (2012) 27.

[23] P. Kanyaboon, T. Saelee, A. Suroengrit, K. Hengphasatporn, T. Rungrotmongkol, W. Chavasiri, S. Boonyasuppayakorn, Cardol triene inhibits dengue infectivity by targeting kl loops and preventing envelope fusion, Sci. Rep. 8 (2018) 16643.

[24] P.P. Wieczorek, N. Hudz, O. Yezerska, V. Horčinová-Sedláčková, M. Shanaida, O. Korytniuk, I. Jasicka-Misiak, Chemical variability and pharmacological potential of propolis as a source for the development of new pharmaceutical products, Molecules 27 (2022) 1600.

[25] B. Trusheva, M. Popova, E.B. Koendhori, I. Tsvetkova, C. Naydenski, V. Bankova, Indonesian propolis: chemical composition, biological activity and botanical origin, Nat. Prod. Res. 25 (2011) 606–613.

[26] M.N. Kardar, T. Zhang, G.D. Coxon, D.G. Watson, J. Fearnley, V. Seidel, Characterisation of triterpenes and new phenolic lipids in Cameroonian propolis, Phytochem. Lett. 106 (2014) 156–163.

[27] N. Pujirahayu, T. Suzuki, T. Katayama, Cycloartane-type triterpenes and botanical origin of propolis of stingless Indonesian bee *Tetragonula sapiens*, Journal 8 (2019) 1–14.

[28] V. Anjaneyulu, K. Ravi, K.H. Prasad, J.D. Connolly, Triterpenoids from *Mangifera indica*, Phytochemistry (Elsevier) 28 (1989) 1471–1477.

[29] E.C. Berghea, M. Craiu, S. Ali, S.L. Corcea, R.S. Bumbacea, Contact allergy induced by mango (*Mangifera indica*): a relevant topic? Méd. 57 (2021) 1240.

[30] L.N. Thanh, H.T. Thoa, N.T.T. Oanh, T.H. Giap, V.T. Quyen, N.T.T. Ha, D.T.L. Phuong, N.T.P. Lien, N.T.M. Hang, Cycloartane triterpenoids and biological activities from the propolis of the stingless bee *Lisotrigona furva*, Vietnam J. Chem. 59 (2021) 426–430.

[31] M. Herrera-López, E. Rubio-Hernández, M. Leyte, A. Schinkovitz, P. Richomme, L. Calvo-Irabién, L. Peña-Rodríguez, Botanical origin of triterpenoids from Yucatecan propolis, Phytochem. Lett. 29 (2019) 25–29.

[32] S. Ma, D. Mandalapu, S. Wang, Q. Zhang, Biosynthesis of cyclopropane in natural products, Nat. Prod. Rep. 39 (2022) 926–945.

[33] J. Salaün, Cyclopropane derivatives and their diverse biological activities, Top. Curr. Chem. 207 (2000) 1–67.

[34] S. Reuter, S.C. Gupta, M.M. Chaturvedi, B.B. Aggarwal, Oxidative stress, inflammation, and cancer: how are they linked? Free Radic. Biol. Med. 49 (2010) 1603–1616.

[35] F. Weinberg, N.S. Chandel, Reactive oxygen species-dependent signaling regulates cancer, Cell. Mol. Life Sci. 66 (2009) 3663–3673.

[36] P.C. Rath, B.B. Aggarwal, *TNF*-induced signaling in apoptosis, J. Clin. Immunol. 19 (1999) 350–364.

[37] S.R. Yan, R.R. Joseph, K. Rosen, M.J. Reginato, A. Jackson, N. Allaire, J.S. Brugge, C. Jobin, A.W. Stadnyk, Activation of *NF-κB* following detachment delays apoptosis in intestinal epithelial cells, Oncogene 24 (2005) 6482–6491.

[38] T. Ittiudomrak, S. Puthong, T. Palaga, S. Roytrakul, C. Chanchao, α-Mangostin and apigenin induced the necrotic death of BT474 breast cancer cells with autophagy and inflammation, Asian Pac. J. Trop. Biomed. 8 (2018) 519–526.

[39] Y.S. Lee, Y.S. Song, R.G. Giffard, P.H. Chan, Biphasic role of nuclear factor-kB on cell survival and *COX-2* expression in SOD1 Tg astrocytes after oxygen glucose deprivation, J. Cerebr. Blood Flow Metabol. 26 (2006) 1076–1088.

[40] C.L. Scaife, J. Kuang, J.C. Wills, D.B. Trowbridge, P. Gray, B.M. Manning, E.J. Eichwald, R.A. Daynes, S.K. Kuwada, Nuclear factor κB inhibitors induce adhesion-dependent colon cancer apoptosis: implications for metastasis, Cancer Res. 62 (2002) 6870–6878.

[41] S. Perego, V. Sansoni, G. Banfi, G. Lombardi, Sodium butyrate has anti-proliferative, pro-differentiating, and immunomodulatory effects in osteosarcoma cells and counteracts the *TNFα*-induced low-grade inflammation, Int. J. Immunopathol. Pharmacol. 31 (2018) 1–14.

[42] E. Amalia, A. Diantini, A. Subarnas, Water soluble propolis and bee pollen of *Trigona* spp. from South Sulawesi Indonesia induce apoptosis in the human breast cancer MCF-7 cell line, Oncol. Lett. 20 (2020) 274.

[43] C.O. da Silva Frozza, T. da Silva Ribeiro, G. Gambato, C. Menti, S. Moura, P.M. Pinto, C.C. Staats, F.F. Padilha, K.R. Begnini, P.M.M.d. Leon, S. Borsuk, L. Savegnago, O. Dellagostin, T. Collares, F.K. Seixas, J.A.P. Henriques, M. Roesch-Ely, Proteomic analysis identifies differentially expressed proteins after red propolis treatment in Hep-2 cells, Food Chem. Toxicol. 63 (2014) 195–204.

[44] P. Hussar, Apoptosis regulators bcl-2 and caspase-3, Encyclopedia 2 (2022) 1624–1636.

[45] G.K. Atkin-Smith, Phagocytic clearance of apoptotic, necrotic, necroptotic and pyroptotic cells, Biochem. Soc. Trans. 49 (2021) 793–804.

[46] W. Park, S. Wei, B.-S. Kim, B. Kim, S.-J. Bae, Y.C. Chae, D. Ryu, K.-T. Ha, Diversity and complexity of cell death: a historical review, Exp. Mol. Med. 55 (2023) 1573–1594.

[47] L.E.E. Chuan-Chun, L.I.N. Meng-Liang, M. Menghsiao, C. Shih-Shun, Galangin induces p53-independent S-phase arrest and apoptosis in human nasopharyngeal carcinoma cells through inhibiting PI3K–AKT signaling pathway, Anticancer Res. 38 (2018) 1377–1389.

[48] H.-M. Wang, C.-C. Chiu, P.-F. Wu, C.-Y. Chen, Subamolide E from *cinnamomum subavenium* induces Sub-G1 cell-cycle arrest and caspase-dependent apoptosis and reduces the migration ability of human melanoma cells, J. Agric. Food Chem. 59 (2011) 8187–8192.